Progress of Theoretical Physics, Vol. 128, No. 4, October 2012

Explosive Nucleosynthesis in Magnetohydrodynamical Jets from Collapsars. II

—— *Heavy-Element Nucleosynthesis of s, p, r-Processes* ——

Masaomi Ono,[1,2,*)] Masa-aki Hashimoto,[2] Shin-ichiro Fujimoto,[3] Kei Kotake[4] and Shoichi Yamada[5]

[1] *Yukawa Institute for Theoretical Physics, Kyoto University, Kyoto 606-8502, Japan*
[2] *Department of Physics, Kyushu University, Fukuoka 812-8581, Japan*
[3] *Kumamoto National College of Technology, Kumamoto 861-1102, Japan*
[4] *Division of Theoretical Astronomy/Center for Computational Astrophysics, National Astronomical Observatory of Japan, Mitaka 181-8588, Japan*
[5] *Advanced Research Institute for Science and Engineering, Waseda University, Tokyo 113-0033, Japan*

(Received March 29, 2012; Revised August 4, 2012)

We investigate the nucleosynthesis in a massive star of 70 $M_\odot$ with solar metallicity in the main sequence stage. The helium core mass after hydrogen burning corresponds to 32 $M_\odot$. Nucleosynthesis calculations have been performed during the stellar evolution and the jetlike supernova explosion of a collapsar model. We focus on the production of elements heavier than iron group nuclei. Nucleosynthesis calculations have been accomplished consistently from hydrostatic to dynamic stages by using large nuclear reaction networks, where the weak *s*-, *p*-, and *r*-processes are taken into account. We confirm that *s*-elements of $60 < A < 90$ are highly overproduced relative to the solar abundances in the hydrostatic nucleosynthesis. During oxygen burning, *p*-elements of $A > 90$ are produced via photodisintegrations of seed *s*-elements. However, the produced *p*-elements are disintegrated in later stages except for ^{180}Ta. In the explosive nucleosynthesis, elements of $90 < A < 160$ are significantly overproduced relative to the solar values owing to the *r*-process, which is very different from the results of spherical explosion models. Only heavy *p*-elements ($N > 50$) are overproduced via the *p*-process because of the low peak temperatures in the oxygen- and neon-rich layers. Compared with the previous study of *r*-process nucleosynthesis calculations in the collapsar model of 40 $M_\odot$ by Fujimoto et al. [S. Fujimoto, M. Hashimoto, K. Kotake and S. Yamada, Astrophys. J. **656** (2007), 382; S. Fujimoto, N. Nishimura and M. Hashimoto, Astrophys. J. **680** (2008), 1350], our jet model cannot contribute to the third peak of the solar *r*-elements and intermediate *p*-elements, which have been much produced because of the distribution of the lowest part of electron fraction in the ejecta. Averaging the overproduction factors over the progenitor masses with the use of Salpeter's IMF, we suggest that the 70 $M_\odot$ star could contribute to the solar weak *s*-elements of $60 < A < 90$ and neutron-rich elements of $90 < A < 160$. We confirm the primary synthesis of light *p*-elements in the ejected matter of high peak temperature. The ejected matter has [Sr/Eu] ~ -0.4, which is different from that of a typical *r*-process-enriched star CS22892-052 ([Sr/Eu] ~ -1). We find that Sr-Y-Zr isotopes are primarily synthesized in the explosive nucleosynthesis in a similar process of the primary production of light *p*-elements, which has been considered as one of the sites of a lighter element primary process (LEPP).

Subject Index: 240, 420, 421, 424, 425

*) E-mail: ono@yukawa.kyoto-u.ac.jp

§1. Introduction

The origin of elements, particularly those heavier than iron, is still under debate.[3] Since charged particle reactions are difficult to produce those elements inside stars because of coulomb barriers, other nucleosynthesis processes, that is, two neutron capture processes, are required. One is the r (rapid)-process and the other is the s (slow)-process.[4] In the r (s)-process, neutron captures are faster (slower) than beta decays. Since the r-process requires high neutron exposure relative to seeds, the r-process favors low electron fraction (Y_e) and/or relatively high-entropy environments.[5]

One of the promising sites of the r-process has been thought to be the neutrino-driven wind.[5)–8] However, recent one-dimensional hydrodynamical simulations of the neutrino-driven wind with Boltzmann neutrino transport have revealed[9] that the electron fraction of the wind becomes high ($Y_e \gtrsim 0.5$) and the entropy becomes low for the r-process. Therefore, other astrophysical sites such as neutron star mergers[10)–12] or black hole winds[13] have been proposed. However, the properties of ejecta such as densities, temperatures, and electron fractions are highly uncertain except for those in Ref. 12), which makes even the qualitative analysis of the r-process difficult.

In general, the s-process occurs at the end of core helium burning in massive stars and/or in AGB stars. Elements heavier than iron of $A < 90$ are produced in massive stars, which is called the weak component of the s-process (weak s-process).[14] On the other hand, elements of $90 < A < 208$ are produced in AGB stars called the main component (main s-process).[14] The s-process is very sensitive to cross sections of neutron captures and β-decay rates, especially at the branching points such as ^{79}Se and ^{85}Kr.[14] Therefore, the nucleosynthesis in massive stars with the use of recent experimental cross sections is worth investigating. From the view point of astrophysics, part of the elements synthesized by the weak s-process could be ejected through the subsequent supernova explosion, where the produced s-elements should be the seeds of the p-process.[15]

Abundances of metal-poor stars provide a good opportunity for understanding the nucleosynthesis because the abundances reflect the outcome only from a small number of supernova explosions. Observations of metal-poor stars have strongly suggested[16] that r-elements of the extremely metal-poor stars that have [Eu/Fe]*) $\gtrsim 1$ (hereafter referred to as r-process-rich stars) have a "universal" abundance pattern, which reproduces the pattern of the solar system r-process abundances for $Z > 56$. However, the abundances of $Z < 56$ are not the case (e.g., Ref. 17)), and the observed [Sr, Y, Zr/Ba, Eu] ratios have dispersion in low-metallicity stars.[18] In particular, on the basis of the models of the chemical evolution of galaxies, it has been suggested[18] that the abundances of Sr-Y-Zr ($Z = 38$, 39, and 40, respectively) estimated from the contributions of the s- and r-processes are about 10 to 20% less than the solar system abundances. As a consequence, a primary component from massive stars is needed to explain 8% of the solar abundance of Sr and 18% of those of Y and Zr, which should require a so-called lighter element primary process

*) We adopt the usual notation $[\mathrm{A/B}] = \log(N_\mathrm{A}/N_\mathrm{A}) - \log(N_\mathrm{A}/N_\mathrm{A})_\odot$ for elements A and B.

(LEPP).[18]

On the other hand, the mechanism of core-collapse supernova explosions is still a topic of debate. Pushed by recent observations revealing the aspherical natures of supernovae,[19),20)] multidimensional studies of core-collapse supernova explosions have been elaborately performed as described in reviews.[21)–25)] Recent two/three-dimensional neutrino-radiation hydrodynamic simulations have shown successful supernova explosions, although in some of the models, the explosion energies are relatively small (10^{49}–10^{50} erg).[26)–29)] QCD phase transition with a mixed phase of quarks and hadrons has also been reported as another possible supernova explosion mechanism even though the explosion is assumed to be spherical.[30)] Magnetohydrodynamical (MHD) simulations with some approximate neutrino transport schemes have shown[31)–35)] jetlike explosions under some specific combinations of initial parameters for a strong magnetic field and differentially rapid rotation. While neutron stars are expected to be left after supernova explosions, it has been suggested that a star of more than 25 $M_\odot$ may collapse to a black hole (BH);[36)] an accretion disk is formed around the BH if the star has enough angular momentum before the collapse. This system could produce a relativistic jet of gamma-ray bursts (GRBs)[37)] due to MHD effects and/or neutrino heating around the rotational axis,[38),39)] whose system is called a collapsar model.[40)] MHD simulations in the context of the collapsar model have shown the formation of jets[41)–48)] due to winding-up effects of the magnetic field or the Blandford-Znajek process.[49)]

Nucleosynthesis calculations of the *r*-process with the use of a collapsar model of 40 $M_\odot$ have been performed extensively by Fujimoto et al.,[1),2)] where it is shown that the *r*-process would operate inside the jets. Explosive nucleosynthesis in GRB jets has also been investigated.[50),51)] Recent nucleosynthesis calculations in a three-dimensional MHD supernova model have suggested that such supernovae could be the sources of the *r*-process elements in the early Galaxy.[52)] However, in those calculations, the produced nuclei are limited to primary synthesized ones inside the jets and comparisons with the solar system abundances have been focused on elements heavier than iron group nuclei. Nucleosynthesis calculations in spherical supernova explosions and detailed hydrostatic ones of the progenitors have proved that elements of $20 < A < 90$ are co-overproduced relative to the solar system abundances.[53)] However, elements of $A > 90$ are not overproduced except for some *p*-elements. Recently, explosive nucleosynthesis calculations for a 15 $M_\odot$ presupernova model[54)] with the solar metallicity based on two-dimensional hydrodynamical simulations have been performed,[55)] in which neutrino-driven explosions are triggered by adjusting the core neutrino luminosity parametrically. They have concluded that the overproductions relative to the solar abundances are similar to the results of spherical explosion models.[53)] In our previous paper (Paper I),[56)] we performed explosive nucleosynthesis calculations inside the jetlike explosions for the collapsar of a 70 $M_\odot$ star with the solar metallicity. These calculations include hydrostatic nucleosynthesis using a nuclear reaction network, which has 464 nuclei (up to ^{94}Kr). In the present paper, we revisit the nucleosynthesis inside the jetlike explosion of the collapsar model and hydrostatic one taking into account all of the weak *s*-, *r*-, and *p*-processes. This makes it possible for us to estimate the consistent abundances of the ejecta. In

particular, we study whether the collapsar model could be the source of elements heavier than iron.

In §2, we present the hydrostatic nucleosynthesis during the evolution from the helium burning stage to the onset of the core collapse. In §3, we briefly summarize the MHD explosion model for the explosive nucleosynthesis and show the results. Section 4 is devoted to a summary of the overall results. We give some discussions with respect to uncertainties and remarks about the connection between metal-poor stars and the possibility for LEPP.

§2. Hydrostatic nucleosynthesis

In Paper I, we investigated the nucleosynthesis in a massive star of 32 $M_\odot$ helium core corresponding to a main sequence star of 70 $M_\odot$.[57] We have used the evolutional tracks with a nuclear reaction network, which includes 464 nuclei (up to ^{94}Kr).[56] In massive stars, the (weak) *s*-process should occur at the end of helium and carbon burning stages. However, in the previous paper, we have included only nuclei of $A < 94$; we could not discuss the weak *s*-process. Therefore, in the present paper, we perform a more detailed nucleosynthesis calculation with a larger nuclear reaction network.

2.1. *Stellar model, initial compositions, and physical inputs*

A star of $M_{\rm ms} \sim 70\ M_\odot$ with the solar metallicity could correspond to the upper limit of accreting BH models (collapsars), because more massive stars suffer from the strong mass loss.[36] As a result, the size of the helium core will be affected considerably by the mass loss. However, the rate of mass loss is still very uncertain;[58] we calculate the evolution of a massive helium core, $M_\alpha = 32\ M_\odot$, without the mass loss as an extreme case, which is worth studying to see the final fate for the series of helium core evolution.

We calculate the nucleosynthesis along each evolutional track of the Lagrange mass from the stage of gravitational contraction of the core to the initiation of iron core collapse. The calculation has been carried out by using changes in the density (ρ), temperature (T) and convective regions. This is the so-called postprocess nucleosynthesis calculation. In convective regions, elements are mixed and compositions become almost uniform. Therefore, the region is calculated as one zone with averaged mass fractions and nuclear reaction rates as in Ref. 59).

Toward *s*-process calculation, we construct a new reaction network including 1714 nuclei up to ^{241}U, in which the reaction rates are based on a new REACLIB compilation, namely, JINA REACLIB database.[60] The included elements are given in Table I. The experimental (n, γ) reaction rates in JINA REACLIB are based on KADoNiS projects.[61] In stellar environments, β-decay rates could be different from the values in laboratories. Takahashi and Yokoi (hereafter referred to as TY87)[62] calculated theoretically the β-decay and electron capture rates for elements heavier than ^{59}Ni and tabulated the rates taking into account thermally enhanced ionized and excited states in stellar interiors. The table ranges over $5{\times}10^7 \leq T \leq 5{\times}10^8$ K and $10^{26} \leq n_e \leq 3{\times}10^{27}$ cm^{-3}, where n_e is the number density of electrons. We adopt

Table I. 1714 nuclides contained in the nuclear reaction network for the hydrostatic nucleosynthesis.

Nuclide	A	Nuclide	A	Nuclide	A	Nuclide	A
H	1 – 3	Cr	46 – 62	Ag	100 – 123	Yb	162 – 184
He	3 – 6	Mn	48 – 65	Cd	103 – 126	Lu	165 – 187
Li	6 – 9	Fe	50 – 68	In	105 – 129	Hf	168 – 189
Be	7 – 12	Co	52 – 70	Sn	108 – 132	Ta	171 – 191
B	8 – 14	Ni	54 – 73	Sb	111 – 135	W	174 – 194
C	9 – 18	Cu	57 – 75	Te	113 – 137	Re	177 – 197
N	11 – 21	Zn	59 – 78	I	117 – 140	Os	180 – 200
O	13 – 23	Ga	62 – 80	Xe	120 – 142	Ir	183 – 203
F	14 – 26	Ge	64 – 83	Cs	122 – 145	Pt	186 – 206
Ne	17 – 28	As	67 – 86	Ba	125 – 148	Au	188 – 209
Na	19 – 30	Se	69 – 89	La	128 – 150	Hg	191 – 212
Mg	21 – 33	Br	72 – 91	Ce	131 – 153	Tl	194 – 215
Al	23 – 35	Kr	74 – 93	Pr	133 – 156	Pb	198 – 217
Si	25 – 38	Rb	76 – 96	Nd	136 – 158	Bi	202 – 220
P	27 – 40	Sr	79 – 98	Pm	138 – 160	Po	205 – 222
S	29 – 42	Y	81 – 101	Sm	141 – 163	At	209 – 224
Cl	31 – 45	Zr	83 – 103	Eu	143 – 165	Rn	212 – 227
Ar	33 – 48	Nb	86 – 106	Gd	146 – 168	Fr	215 – 229
K	35 – 50	Mo	89 – 109	Tb	148 – 171	Ra	217 – 232
Ca	37 – 53	Tc	91 – 112	Dy	151 – 174	Ac	222 – 234
Sc	39 – 55	Ru	93 – 115	Ho	154 – 176	Th	225 – 237
Ti	41 – 57	Rh	96 – 117	Er	157 – 179	Pa	227 – 239
V	43 – 59	Pd	98 – 120	Tm	160 – 181	U	231 – 241

the temperature and density dependence of the rates if available. Unfortunately, the range of the table is limited only for T and ρ of the helium burning stage. If the temperature and density are outside of the table, we use the values of the edges of the table. Reaction rates concerning ^{180}Ta are specially treated as noted in Appendix A, because ^{180}Ta has a long-lived isomeric state. As suggested by Prantzos et al.,[59] the timescales of neutron-induced reactions ($\approx 10^{-4}$ s) are much shorter than those of the variation of abundances of the other elements ($\approx 10^{9}$–10^{11} s) as well as convective timescales, and thereby, neutron abundance is determined locally under thermal equilibrium conditions. This indicates that neutrons are not mixed uniformly in convective regions. Therefore, to calculate abundances in a convective region as one zone including the effects of different neutron abundances over the region, we adopt doubly averaged reaction rates for "neutron-induced" reactions of (n,γ), (n,p), and (n,α), according to the same method described in Ref. 59).

Let $X(i)$ denote the mass fraction of the element i. The initial mass fractions are assumed to be $X(^4\mathrm{He}) = 0.981$ and $X(^{14}\mathrm{N}) = 0.0137$, where all the original CNO isotopes are assumed to be converted to ^{14}N during the core hydrogen burning. Mass fractions of the heavier elements are taken to be proportional to the solar system abundances[63] (e.g., $X(^{56}\mathrm{Fe}) = 1.17 \times 10^{-3}$).

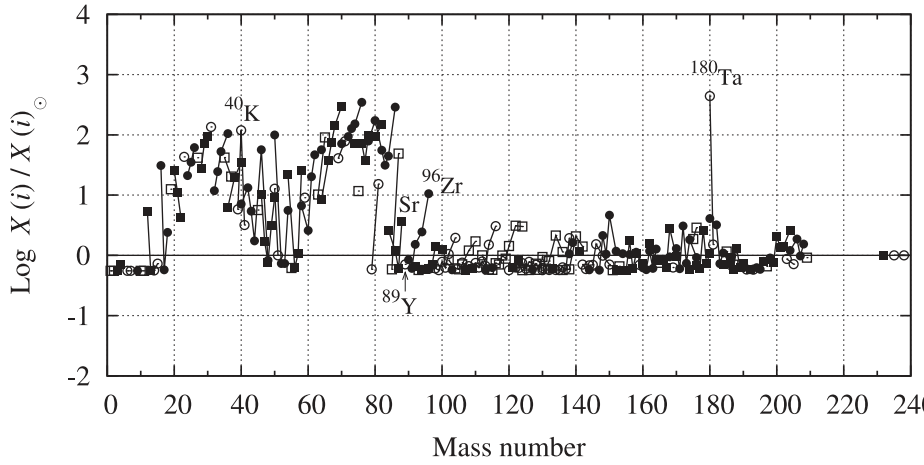

Fig. 1. Overproduction factors $X(i)/X(i)_{\odot}$ against the mass number A averaged over the star including the hydrogen envelope at the beginning of the core collapse. Distinguished symbols connected by lines indicate the isotopes.

The evolutionary changes in composition with respect to the stellar structure such as ^{12}C, ^{16}O, and ^{20}Ne are slightly different from the results with the use of the reaction network of 464 nuclei[56] originating from the differences in the initial abundances and adopted reaction rates. The produced mass fractions of elements of $A > 94$, which have not been included in the 464 network, amount to about 10^{-6}. Therefore, differences of 10^{-6} in mass fractions may be introduced. Although there are some differences in the main composition as described in Paper I between the original stellar evolution model[57] and postprocess hydrostatic nucleosynthesis calculations with the reaction network of 464 or 1714 nuclei, the differences are not so large for our purpose.

2.2. *S- and p-processes*

Let us focus on the production of elements heavier than iron and the weak *s*- and *p*-processes in the hydrostatic nucleosynthesis. Figure 1 shows overproduction factors $X(i)/X(i)_{\odot}$ at the beginning of the core collapse, where $X(i)$ is the value averaged over the star including the hydrogen-rich envelope of 38 $M_{\odot}$, and $X(i)_{\odot}$ is that of the solar system abundances. It is noted that in the estimation of the overproduction factors, we adopt the value of 4.55×10^9 yr ago for ^{40}K, which is a long-lived radioactive nucleus (the half-life is 1.25×10^9 yr) and the present abundance is about one order of magnitude less than that when the solar system was born (~ 4.5 yr ago). There is inconsistency between the initial abundance of ^{40}K and the value in the estimation of the overproduction factor. However, the overproduction of ^{40}K is not determined by the initial abundance of ^{40}K but by the abundance of ^{39}K as described below. Overall, elements of $60 < A < 90$ are highly overproduced relative to the solar ones; the overproduction level ranges over 10^2 – 10^3, which is similar to the weak *s*-process scenario proposed by many previous studies of the *s*-process in massive stars.[59),64),65)]

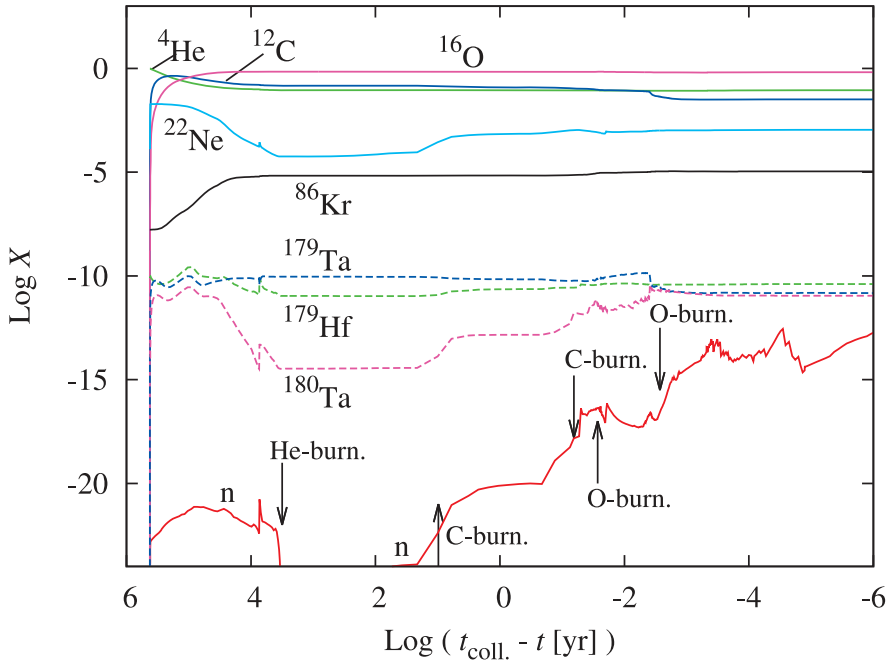

Fig. 2. Changes in mass fractions of selected elements averaged over the helium core against remaining time before the core collapse ($t_{\rm coll.} = 4.22\times10^5$ yr). Upward (downward) arrows denote the time of the start (end) of the burning stages.

Figure 2 shows the time evolution of mass fractions of selected elements averaged over the whole star. ^{86}Kr, which is one of the representative s-elements, is overproduced at the helium burning stage. We confirm that the overproduced elements of $60 < A < 90$ are mainly produced during the helium core burning, and the neutrons are mainly supplied by the ^{22}Ne$(\alpha, n)^{25}$Mg reaction (Fig. 2) as pointed out in previous studies (see Ref. 14) for a recent review). ^{22}Ne is produced by the sequence of ^{14}N$(\alpha,\gamma)^{18}$F$(\beta^-\nu)^{18}$O$(\alpha,\gamma)^{22}$Ne reactions. ^{40}K is produced by the ^{39}K$(n,\gamma)^{40}$K reaction in the helium burning stage. The solar system abundances of ^{39}K and ^{40}K are 3516 and 0.44 (the present value) (normalized as the abundance of silicon to be 10^6),[63] respectively. Therefore, even if the small amount of ^{39}K is converted to ^{40}K, we regard it to be much overproduced relative to the solar value. ^{180}Ta is also overproduced in the helium burning stage by the sequence of ^{179}Hf$(\beta^-)^{179}$Ta$(n,\gamma)^{180}$Ta reactions (see Fig. 2). It is noted that the reaction channel of ^{179}Hf$(\beta^-)^{179}$Ta is closed if we do not use the β-decay rates of TY87 because ^{179}Hf is stable in the laboratory. However, overproduced ^{180}Ta decays from a thermally populated ground state at the end of the helium burning, and the overproduction level returns almost to the initial value (Fig. 2). In the helium burning stage, ^{96}Zr is overproduced more than 10 times (Fig. 1) relative to the solar value by neutron captures, which are faster than β^--decays of ^{95}Zr ($\tau_{1/2} \sim 64$ d). However, Sr and Y are not so overproduced. Although the overproduction levels of the elements of $10 < A < 90$ do not increase

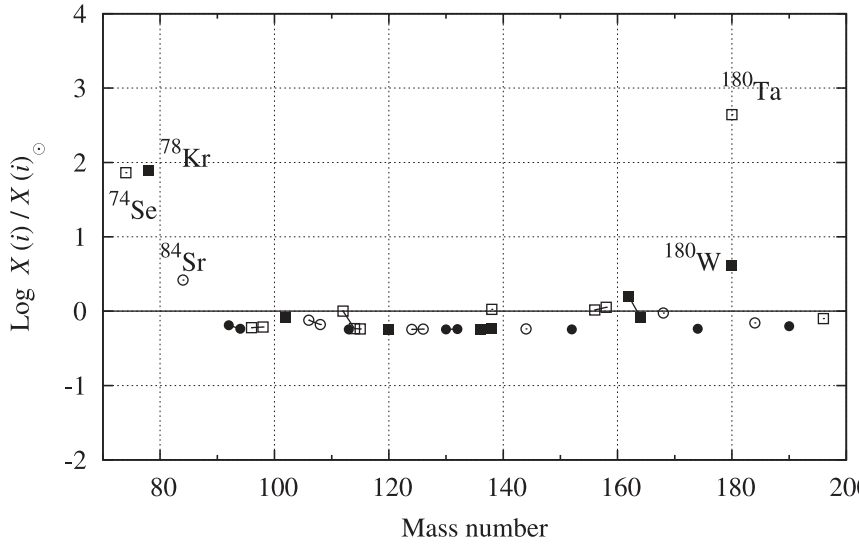

Fig. 3. Same as Fig. 1 but for 35 p-elements.

significantly after the helium burning, some elements of $A > 90$ are produced after that.

In the carbon and neon burning stages, neutrons are mainly supplied by reactions of $^{12}\mathrm{C}(^{12}\mathrm{C},n)^{23}\mathrm{Mg}$, $^{13}\mathrm{C}(\alpha,n)^{16}\mathrm{O}$, $^{17}\mathrm{O}(\gamma,n)^{16}\mathrm{O}$, and $^{25}\mathrm{Mg}(\alpha,n)^{28}\mathrm{Si}$. The $^{22}\mathrm{Ne}(\alpha,n)^{25}\mathrm{Mg}$ reaction is also activated in the helium burning shell. Since ^{179}Hf is produced by neutron captures, ^{180}Ta is overproduced again relative to the solar value via the sequence of $^{179}\mathrm{Hf}(\beta^-)^{179}\mathrm{Ta}(n,\gamma)^{180}\mathrm{Ta}$.

During the oxygen burning stage, the temperature becomes high ($T_\mathrm{c} \sim 2{\times}10^9$ K, where T_c is the temperature at the center) and photodisintegrations of s-elements activate the p-process in the oxygen- and neon-rich layers. The possibility of the p-process in hydrostatic evolution of massive stars was proposed in previous studies.[53),66)–68)] We find that seed s-elements that have larger mass numbers tend to be disintegrated into p-elements by (γ,n) reactions, and light p-elements of ^{74}Se, ^{78}Kr, and ^{84}Sr are produced at the oxygen- and neon-rich layers by (γ,n) and (γ,p) reactions (Fig. 3). It is noted that ^{180}Ta is produced more and more by the $^{181}\mathrm{Ta}(\gamma,n)^{180}\mathrm{Ta}$ reaction. Since the solar abundances of ^{180}Ta are much smaller than those of ^{181}Ta, conversion of small amounts of ^{181}Ta leads to the overproduction of ^{180}Ta relative to the solar value.

In the later stages, produced p-elements of $A > 90$ are disintegrated by subsequent (γ,n) reactions and β^+-decays except for ^{180}Ta. After all, p-elements whose overproduction factors are greater than 10 are only ^{74}Se, ^{78}Kr, and ^{180}Ta at the beginning of the collapse (see Fig. 3). It is noted that (n,γ) and (γ,n) reactions are in thermal equilibrium at this stage.

The quantitative assessment of the adopted beta decay rates (TY87) should require more experimental data.[14)] Moreover, the table of the β-decay rates of TY87 covers only the temperature and density of the helium burning stage as mentioned in

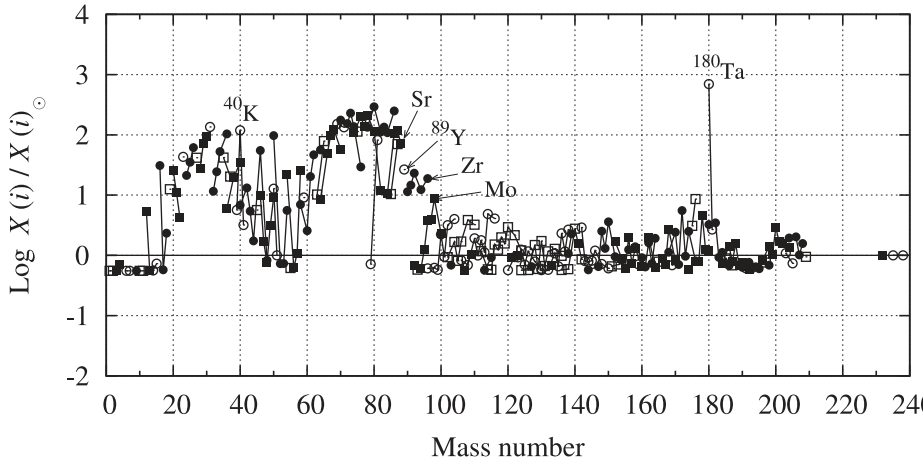

Fig. 4. Same as Fig. 1 but for the results with use of laboratory β-decay rates instead of those of TY87.

§2.1. Therefore, we have also calculated the nucleosynthesis using laboratory β-decay rates instead of those of TY87. Although overall overproduction levels change only by some factors as seen in Fig. 4, those of more neutron-rich isotopes of $60 < A < 85$ tend to be decreased. We find that the production of elements for $85 < A < 100$ is very sensitive to the differences in β-decay rates, and Sr, Y, Zr, and Mo tend to be overproduced. Although the channel of $^{179}\mathrm{Hf}(\beta^-)^{179}\mathrm{Ta}(n,\gamma)^{180}\mathrm{Ta}$ is closed without TY87, ^{180}Ta is produced by the $^{181}\mathrm{Ta}(\gamma,n)^{180}\mathrm{Ta}$ reaction after the carbon burning and remains through $(n,\gamma) \rightleftharpoons (\gamma,n)$ equilibrium in the later stages.

Let us summarize the hydrostatic nucleosynthesis. 1) We confirm the weak s-process scenario: s-elements of $60 < A < 90$ are highly overproduced relative to the solar abundances. 2) High overproductions of ^{180}Ta could be attributed to the higher density and temperature evolutional tracks of the 70 $M_\odot$ star. 3) The p-process in the oxygen- and neon-rich layers occurs after the carbon burning stage. However, the produced p-elements do not remain due to subsequent (γ,n) reactions and β^+-decays. We suggest that for smaller massive stars, the overproductions of ^{180}Ta are significantly decreased because of the lower density and temperature evolutional paths. On the other hand, the p-process could become important because the produced p-elements of larger mass numbers may survive in low-density and low-temperature environments.

§3. Explosive nucleosynthesis in a magnetohydrodynamical jet

In Paper I, we investigated the explosive nucleosynthesis with the nuclear reaction network including 464 nuclei (up to ^{94}Kr).[56] In the present paper, we recalculate the explosive nucleosynthesis with a much larger reaction network and focus on the production of heavier elements, that is, p- and r-elements. In this section, we present the review of the explosion model, the method of explosive nucleosynthesis, and the results combined with that of the hydrostatic nucleosynthesis.

3.1. *Supernova explosion model*

In Paper I, we have constructed supernova explosion models using a collapsar model.[56] Here, we briefly summarize the explosion model for the nucleosynthesis calculation. We have performed two-dimensional MHD simulations of the collapsar model using a nonrelativistic MHD code, ZEUS-2D,[69),70] which is modified[71] for handling supernova simulations with a realistic nuclear equation of state (EOS) based on the relativistic mean field theory.[72]

For a low-density region of $\rho < 10^5$ g cm^{-3}, another EOS is connected[73] smoothly at the density boundary, which consists of the nonrelativistic ions, partially degenerate relativistic electrons, and radiation.

We have taken into account neutrino cooling by electron-positron ($e^{\pm}$) pair captures on nucleons, $e^{\pm}$ pair annihilation, and nucleon-nucleon bremsstrahlung. We neglect to include both detailed neutrino transport and heating processes, because the maximum density remains less than 10^{10} g cm^{-3} in our calculations. We discuss the effects of neutrino absorptions on the nucleosynthesis in §3.2. BH was mimicked as an inner free absorption boundary and gravitational point source with pseudo Newtonian potential.[74] We adopted the spherical coordinate (r, θ, ϕ), and the computation domain was taken from the inner boundaries $r_{\rm in} = 50$ – 200 km to $3{\times}10^4$ km, which covers inner oxygen-rich layers.

The initial presupernova model is the 32 $M_\odot$ helium core corresponding to an $M_{\rm ms} = 70$ $M_\odot$ star,[57] which is the same stellar evolution model obtained in the previous section. The initial configuration of angular velocity and magnetic field was implemented by analytical form with parameters as in the previous study.[2),31),43),44] The initial angular velocity is written as follows:

$$\Omega\,(r) = \Omega_0 \frac{r_0^2}{r^2 + r_0^2}, \tag{3·1}$$

where r is the radius from the center, and Ω_0 and r_0 are model parameters. The initial toroidal magnetic field is given in proportion to the angular velocity distribution as

$$B_\phi\,(r) = B_0 \frac{r_0^2}{r^2 + r_0^2}, \tag{3·2}$$

where B_0 is a model parameter. We adopt the R51 model as in Paper I for the explosive nucleosynthesis, which has the largest amount of the mass end energy ejection rates among the investigated models. The parameters of the initial angular velocity and magnetic field are $\Omega_0 = 5$ s^{-1}, $r_0 = 1500$ km, $B_0 = 5.7 \times 10^{12}$ G, and $B_Z = 5 \times 10^{11}$ G, where B_Z is the initial uniform poloidal magnetic field along the rotational axis. The specified parameters of the rotation and magnetic field correspond to the model of the rapid rotation and the strong magnetic field. Recent stellar evolution models indicate[75] that if the magnetic field is taken into account, the resultant specific angular momentum of the central region becomes smaller than that required for the typical collapsar model ($j \sim 10^{17}$ cm^2 s^{-1} [37]). In our simulation, the jet is triggered by the central magnetic pressure, which grows due to the compression and winding-up effects of the magnetic field, and the amplified magnetic field reaches around $\sim 10^{15}$ G. If the magnetorotational instability (MRI)[76]

successfully operates in the core-collapse phase, the magnetic field could be quickly amplified to the same level from an initial magnetic field weaker than that ascribed in the present paper. However, resolving MRI in a global simulation is very hard and not feasible in the present calculations. Therefore, we assume that some mechanisms such as MRI amplify the magnetic field rapidly from a weak initial magnetic field and we mimic the situation by simply imposing a strong initial magnetic field. Note that the reached magnetic field strength $\sim 10^{15}$ G is comparable to that at saturation due to MRI.[77)]

The resulting total ejection mass and explosion energy at the end of the simulation ($t_f = 1.504$ s) are 0.124 $M_\odot$ and 3.02×10^{50} erg, respectively. The specific angular momentum j after the formation of a disklike structure is about 5×10^{16} cm^2 s^{-1} at the radius of 500 km. The disk extends to about 1000 km from the center at the accretion phase. After the strong jet formation, an expanding bow shock is generated at the outer region of the disk and the matter residing in the region begins to expand outward along the equatorial axis (see the description of Fig. 5 in §3.2). However, even after the formation of the jet and the expanding bow shock, the accretion continues at the inner edge of the disk and the accretion rate maintains the value of 0.1 – 1 $M_\odot$ s^{-1} with a few factors declined in 1 s. Therefore, our model can be regarded as a collapsar model. It is noted that the jet obtained by the simulation is mildly relativistic ($\lesssim 0.1\ c$) and baryon rich ($\gtrsim 0.1\ M_\odot$). In contrast, ultrarelativistic GRB jets should be baryon poor ($\sim 10^{-5}\ M_\odot$[78)]). Moreover, the event rate of mildly relativistic jets could be larger than those of normal GRB jets.[79)] Therefore, both the ejected mass and event rate suggest that the contribution to the chemical evolution of galaxies could be large compared with that of ultrarelativistic ones.

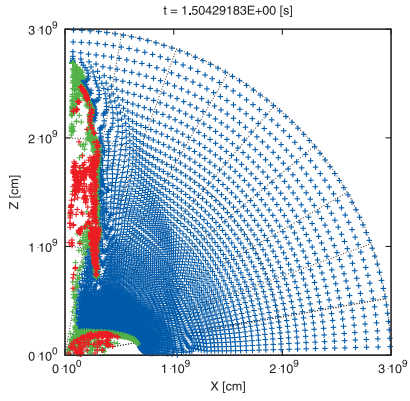

Fig. 5. Distribution of the tracer particles on the XZ-plane at the end of the simulation ($t_f = 1.504$ s). The particles initially located at the inner iron core, Si-rich layers and oxygen-rich layers are indicated in red, green, and blue, respectively.

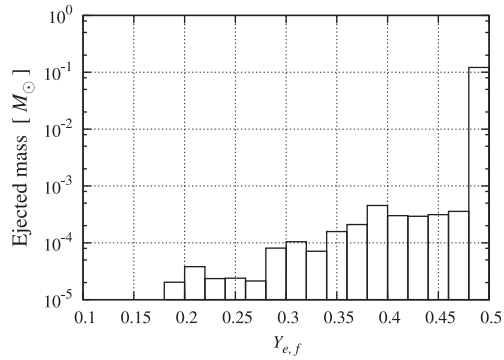

Fig. 6. Ejected masses against electron fraction at the end of NSE stage.

3.2. *Computational method of nucleosynthesis inside the jet*

For calculating the nucleosynthesis inside the MHD jet, 20,000 tracer particles are distributed over the computational domain between 1000 km and 3×10^4 km from the center, which covers initially the region from around the iron core surface to the inner oxygen-rich layer. All the matter initially located at radii smaller than 1000 km is absorbed into the inner boundary. The Lagrange evolution of density and temperature of each tracer particle can be obtained from the method described in Refs. 80) and 1), by which we calculate the nucleosynthesis and follow the change in composition. Figure 5 shows the distribution of the tracer particles at the end of the simulation ($t_f = 1.504$ s). The particles initially located at the inner iron core, Si-rich layers, and oxygen-rich layers are indicated in red, green, and blue, respectively. Some fractions of the particles initially located at the inner iron core are ejected by the jet. It should be noted that in Fig. 5, we can see a "blank" region in which there are no particles in the equatorial regions. The blank region corresponds to the expanding region after the jet formation as mentioned in §3.1. The density of the equatorial blank region is $\rho \lesssim 10^5$ g cm^{-3}. In the tracer particle method, the distributions of the particles tend to be sparse in expanding and low-density regions. We can also see relatively sparse regions in polar regions. The blank is just the problem of the tracer particle method and the region does not affect the nucleosynthesis outcome in the ejecta. Additionally, we have performed a convergence test of the nucleosynthesis results inside the jet by changing the number of distributed particles and confirmed that the results are not changed much by the difference in Paper I. Particles that appear deep inside the original iron core go through high-density and high-temperature regions; if the temperature is greater than 10^{10} K, the compositions are determined under nuclear statistical equilibrium (NSE) condition: they are obtained from the values of (ρ, T, Y_e). Since these particles suffer from electron captures, we need to calculate the change in Y_e of the ejected tracer particles due to the weak interactions of $e^{\pm}$ captures and $\beta^{\pm}$ decays until the last stage of NSE before the network calculation. The change in Y_e is given by[81]

$$\frac{dY_e}{dt} = \sum_i (\lambda_+ - \lambda_-) y_i, \tag{3·3}$$

where λ_+ represents the β^- and positron capture rates and λ_- represents the β^+ and electron capture rates. Figure 6 shows the distribution of the ejected mass in $M_\odot$ against the electron fraction of ejected particles at the end of NSE ($Y_{e,f}$). After the end of NSE, the nucleosynthesis calculation is done along the Lagrange evolution of each particle by using a large nuclear reaction network. Since the time of hydrodynamical simulation is insufficient to follow the decays of radioactive nuclei, the density and temperature profiles of particles are extrapolated assuming adiabatic expansion as in Refs. 1) and 56). We continue the nucleosynthesis calculation of the radioactive decays until $\sim 10^{10}$ yr after the explosion. Note that we neglect the feedback of energy generations due to nuclear processes such as photodisintegrations in the hydrodynamical calculation because our nucleosynthesis calculations are just postprocessing. The effects of neutrino absorptions on the evolution of Y_e should be

noted here because we neglect the effects in the nucleosynthesis calculations, but it could be critical for the nucleosynthesis outcome. The inner edge of the accretion disk of the R51 model has $\rho \sim 10^9$ g cm^{-3} and the estimated neutrino luminosity ranges from $\sim 10^{51}$ to $\sim 10^{52}$ erg s^{-1}, which is about one order of magnitude smaller than that of canonical core-collapse supernovae. Therefore, the neutrino absorptions could not be effective. Note that the range of the neutrino luminosity does not differ much from that of other models in Paper I. Additionally, although the progenitor and specified initial angular momentum and magnetic field distributions differ from that of our model, recent nucleosynthesis calculations in a magnetorotationally driven core-collapse supernova model with an approximate neutrino transport scheme including effects of neutrino absorptions on Y_e have revealed[52] that the peak distribution of Y_e in the ejecta is shifted from ~ 0.17 to ~ 0.15 between with and without neutrino absorptions, but the results of the nucleosynthesis are not much affected by the difference. From the above considerations, the effects of neutrino absorptions on Y_e in our model would be small and we neglect the effects.

To investigate the heavy-element nucleosynthesis including the *p*- and *r*-processes, we calculate the nucleosynthesis along some Lagrange tracks of the ejected particles explained above using the large nuclear reaction network[81] including 4463 nuclei (up to ^{292}Am), where the reaction rates are mainly based on the REACLIB database[82),83] and the adopted theoretical mass formula is the extended Thomas-Fermi plus Strutinsky integral (ETFSI).[84] It is noted that the reaction rates in the hydrostatic nucleosynthesis calculations are based on the JINA REACLIB database, which use the theoretical mass formula of the finite-range droplet model (FRDM).[85] Therefore, there could be some inconsistency between the hydrostatic and explosive nucleosynthesis calculations. However, taking into account the marked uncertainty of the reaction rates far from the valley of the nuclear stability, the differences are acceptable in the present purpose.

3.3. *P- and r-processes*

To investigate the total yield of the ejecta, we combine the results of the hydrostatic and explosive nucleosyntheses. We assume that all the unshocked matter located at larger radii than the jet front in the star (including the hydrogen envelope) of $\theta < 15^\circ$ is successfully ejected by the jet, keeping the precollapse compositions unchanged.

As shown in Fig. 6, the mass distribution of the ejecta tends to decrease as the electron fraction $Y_{e,f}$ decreases. The lowest value of $Y_{e,f}$ is 0.192 among the ejected particles. We find that the low-$Y_{e,f}$ particles are ejected from deep inside the disk, which are originally located from the edge of the iron core to the inner Si-rich layer and fall into near the BH due to gravitational collapse. The low-$Y_{e,f}$ particles strongly suffer from electron captures, which reduces the electron fractions of the particles. The distributions of compositions of the particles are initialized by the final state in NSE. On the other hand, the particles that do not suffer from nuclear burning are just pushed up by the inner jet at larger radii. Such particles maintain the precollapse compositions. Therefore, the precollapse abundances are crucial in part to determine the total compositions of the ejected matter.

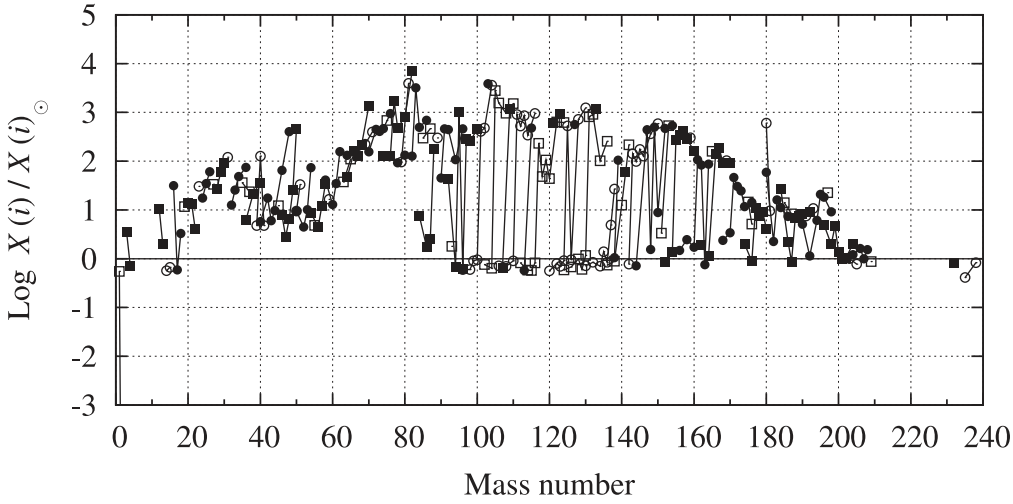

Fig. 7. Same as Fig. 1 but for the ejecta with the use of the larger network.

The final overproduction factors $X(i)/X(i)_{\odot}$ averaged over the ejecta against the mass number are shown in Fig. 7. Symbols connected by lines indicate the isotopes. Note that neutron-rich elements of $45 < A < 55$ and $60 < A < 160$ are highly overproduced relative to the solar values. Figure 8 shows the abundances of ejected particles that have different electron fractions at the end of the NSE stage. The overproduced elements of $140 < A < 200$ originate from the ejected matter, which has a lower $Y_{e,f}$ of around 0.2 (Fig. 8), where the ejected materials undergo r-process nucleosynthesis. On the other hand, the ejected particles of $Y_{e,f} \sim 0.3$ produce elements of $60 < A < 90$. The overproduced elements of $A > 90$ are primarily synthesized in the jet except for ^{180}Ta. The overproduction factors have a peak at $A = 195$ (the neutron magic number of 126). It should be noted that our jet model cannot considerably produce the elements around the third peak. In contrast, they are significantly produced in the study by Fujimoto et al.,[1),2)] which is attributed to the different distribution of the lowest part of $Y_{e,f}$ of ejecta. In Fujimoto et al., the particles with $Y_{e,f} \sim 0.1$ are also ejected from their collapsar model of 40 $M_{\odot}$ (see e.g., Fig. 5 in Ref. 2)). Since the lowest $Y_{e,f}$ is about 0.2 in our model, strong r-process and fissions do not proceed. The difference in the distribution of $Y_{e,f}$ may be ascribed to those of the progenitors and implemented initial distributions of the angular momentum and the magnetic field. In particular, we include the initial toroidal magnetic field, which may inhibit matter to fall deep inside the core and suffer from strong electron captures.

S-elements of $60 < A < 90$ are overproduced significantly, which is due to the weak s-process in the hydrostatic evolutional stage. In contrast, no s-elements of $A > 90$ are overproduced, which might be compensated by the products of the main s-process in the relatively low mass AGB stars.

The overproduction factors of 35 p-elements are shown in Fig. 9. P-elements whose overproduction factors are greater than 10 are ^{74}Se, ^{78}Kr, ^{84}Sr, ^{92}Mo, ^{180}Ta,

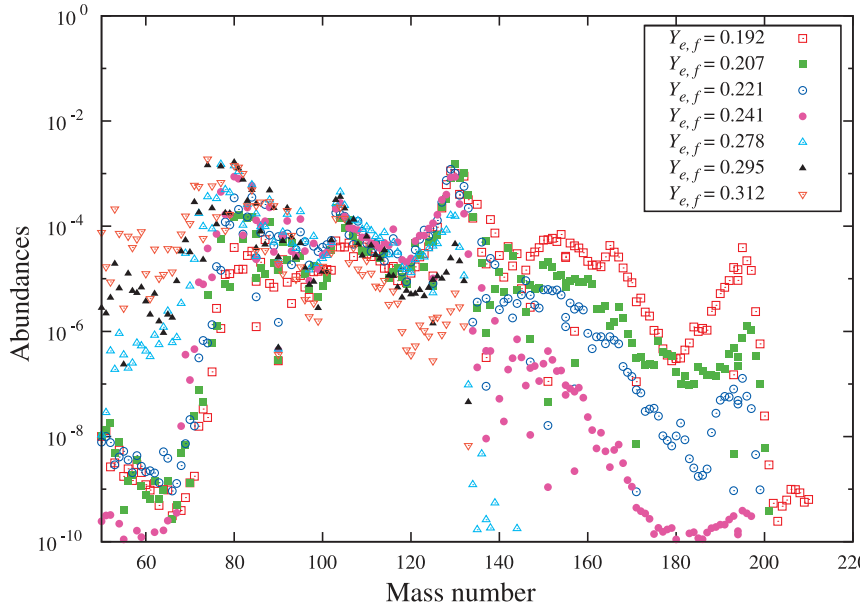

Fig. 8. Abundances of ejected particles with $Y_{e,f}$ that have different electron fractions at the end of NSE stage.

^{180}W, ^{184}Os, ^{190}Pt, and ^{196}Hg. On the other hand, *p*-elements of ^{74}Se, ^{78}Kr, ^{84}Sr, ^{180}W, and ^{180}Ta are overproduced in the hydrostatic nucleosynthesis (see Fig. 3); those of ^{92}Mo, ^{184}Os, ^{190}Pt, and ^{196}Hg are mainly overproduced in explosive nucleosynthesis. Underproduced *p*-elements in the previous study of the *p*-process in Type II supernovae[15] such as ^{94}Mo and ^{96,98}Ru are not produced in our explosion model. Rayet et al.[15),86] have investigated the *p*-process (gamma process) in parametrized supernova explosion models. They concluded that the production of *p*-elements is very sensitive to the maximum temperature reached during the explosion, and the light ($N \lesssim 50$), intermediate ($50 \lesssim N \lesssim 82$) and heavy ($N \gtrsim 82$) *p*-elements are produced in the peak temperature classified as $T_{9,\max} \gtrsim 3$, $3 \gtrsim T_{9,\max} \gtrsim 2.7$, $2.5 \gtrsim T_{9,\max}$, respectively, where $T_9 = T/(10^9\,\mathrm{K})$. The mass distribution against the peak temperatures of the ejecta initially located in the oxygen- and neon-rich layers is shown in Fig. 10. The major part of the ejected matter has $T_{9,\max} \lesssim 2.5$. Thereby, heavy *p*-elements are considerably produced in the explosive nucleosynthesis (Fig. 9). It is emphasized that light *p*-elements of ^{74}Se, ^{78}Kr, ^{84}Sr, and ^{92}Mo are primarily synthesized in the ejecta of $T_{9,\max} \sim 16$ and $Y_{e,f} \sim 0.48$ initially located in Si-rich layers. Since the peak temperature is very high, protons, neutrons and alpha particles are significantly produced by photodisintegrations of heavy nuclei, and the light *p*-elements are produced by a sequence of neutron captures and subsequent proton captures as described in Fujimoto et al.,[1] the scenario of which was originally proposed by Howard et al.[87] Since light *p*-elements are already produced in the hydrostatic nucleosynthesis, the increments due to the primary process in the explosive nucleosynthesis are not prominent except for ^{92}Mo. Note that in Fujimoto

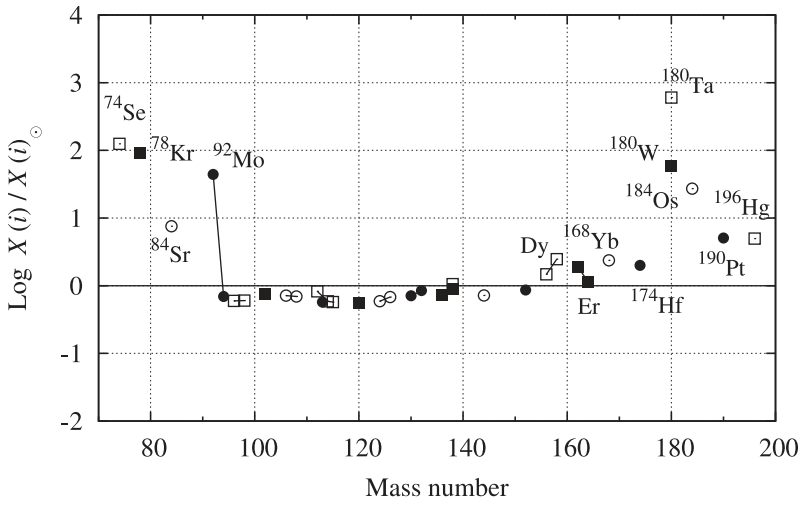

Fig. 9. Same as Fig. 7 but 35 p-elements.

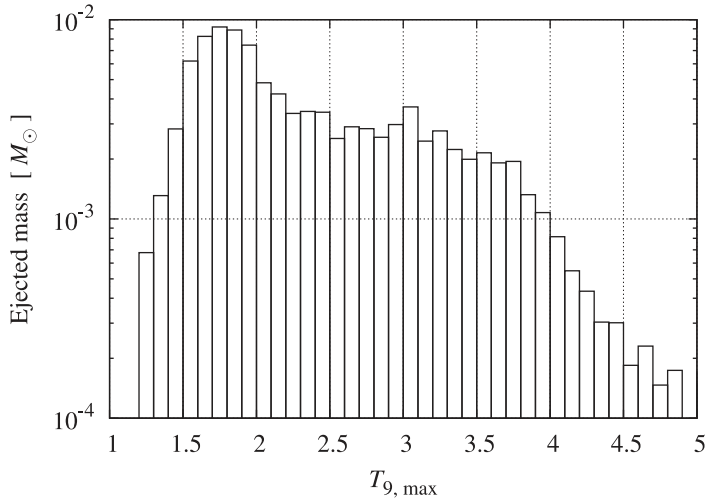

Fig. 10. Ejected mass originated from initial oxygen- and neon-rich layers against the peak temperature $T_{9,\,\mathrm{max}}$ ($T_9 = T/(10^9\mathrm{K})$).

et al.,[1)] intermediate p-elements such as ^{133}In, ^{115}Sn, and ^{138}La are also produced by fission only in the ejecta of $Y_{e,f} \sim 0.1$. In our model, all the ejected matter has $Y_{e,f} \gtrsim 0.2$; therefore, fission reactions are not effective and intermediate p-elements cannot be produced.

§4. Summary and discussion

We have investigated the nucleosynthesis in a massive star of 32 $M_\odot$ helium core with solar metallicity during the stellar evolution and the jetlike supernova

explosion. In this section, we summarize the results and discuss the uncertainties of the production of elements and contribution to the chemical evolution of galaxies (§4.1). We also give additional discussion by comparing with observations in §4.2.

Hydrostatic nucleosynthesis: 1) *S*-elements of $60 < A < 90$ are highly overproduced relative to the solar abundances, which is similar to the weak *s*-process scenario proposed in previous studies.[59),64),65)] 2) Although photodisintegrations of seed *s*-elements during oxygen burning produce *p*-elements, the produced elements are disintegrated in the later stages except for ^{180}Ta. 3) Three elements, Sr, Y, and Zr, are not much overproduced compared with the solar values except for ^{96}Zr.

Explosive nucleosynthesis: 4) Elements of $90 < A < 160$ are significantly overproduced relative to the solar values. 5) The overproduced elements of $140 < A < 200$ originate from the ejected matter with lower $Y_{e,f}$ around 0.2, which results in the *r*-process. 6) The *p*-process produces mainly heavy *p*-elements ($N > 50$) because the peak temperatures in the oxygen- and neon-rich layers are relatively low. 7) Light *p*-elements are produced as primary ones in the ejected matter, which has a high peak temperature. 8) Compared with the previous study of *r*-process nucleosynthesis calculations in a collapsar model of 40 $M_\odot$ by Fujimoto et al.,[1),2)] our jet model cannot considerably produce both the elements around the third peak of the solar *r*-elements and intermediate *p*-elements. This may be attributed to the differences in the progenitor and the specified initial angular momentum and magnetic field distributions.

After all, our supernova explosion model results in neutron-rich elements of $70 < A < 140$ and weak *s*-elements of $60 < A < 90$. The origin of other underproduced elements would be ascribed to different explosion mechanisms of supernovae.

Here, we try to deduce the qualitative constraint on the event rate for our explosion model. Let us assume canonical supernova explosion to be spherical and/or neutrino-driven aspherical ones such as in Refs. 53) and 55). The overproduction levels for the elements of $60 < A < 160$ are 1 – 2 orders of magnitude higher than that for those of $20 < A < 60$ compared with canonical ones. If we neglect the mass loss, the total ejected mass of our jetlike explosion model is around 2 $M_\odot$, which is about one order of magnitude less than that of canonical ones. Unless the event rate of our model is comparable to or one order of magnitude less than that of canonical ones, the elements of $60 < A < 160$ are too produced to explain the solar system abundance pattern. Therefore, the event rate of our model could be one order of magnitude less than that of canonical ones. The origin of other underproduced elements would be ascribed to different types of supernovae. However, the constraint speculated here is not strict.

4.1. *Uncertainties of production of elements related to the chemical evolution of galaxies*

We discuss the uncertainties concerning overproductions. To investigate the weak *s*-process in the hydrostatic nucleosynthesis, we adopt β-decay rates of TY87. However, the table of the rates for ρ and T only covers the temperature and density ranges in the helium burning stage. As noted in §2.2, we find that productions of neutron-rich elements of $85 < A < 100$, in particular, Sr, Y, Z, and Mo, are very

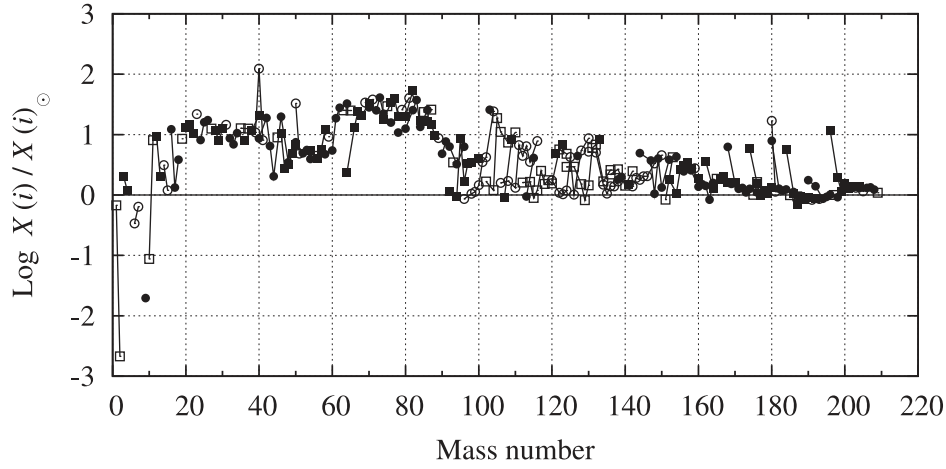

Fig. 11. Same as Fig. 1 but for averaged over progenitor masses weighed on the basis of Salpeter's IMF with the use of spherical explosion models from Rauscher et al. for 15, 19, 20, 21, 25, 30, 35, and 40 $M_\odot$ progenitors and our explosion model for 70 $M_\odot$.

sensitive to the adopted β-decay rates. Therefore, it is urgent to construct a table of the β-decay rates, which covers all evolutional stages.

In the explosive nucleosynthesis calculation, we use the theoretical reaction rates based on ETFSI mass formula for elements far from the valley of the nuclear stability, in which no experimental cross sections are available. The produced abundance pattern should depend on an adopted mass formula.[1)]

We assume that all the matter that has larger radii than the jet front in the star of $\theta < 15^\circ$ is successfully ejected by the jet. However, the angle from which the matter should be ejected is rather uncertain. Although we neglect the effects of the mass loss, a star of 70 $M_\odot$ with solar metallicity should suffer from a significant mass loss.[36)] If the mass loss is effective, almost all the hydrogen-rich envelope should be ejected as the stellar wind. If the above uncertainties are taken into account, the overproduction levels could become one order of magnitude less than those described in the previous sections. However, the overall abundance patterns do not change qualitatively except for the overproduction levels.

To investigate the possible contribution of our explosion model to the chemical evolution of galaxies, we estimate overproduction factors averaged over progenitor masses weighted on the basis of Salpeter's stellar initial mass function (IMF).[88)] The IMF averaged overproduction factor of the element i, $f_{\rm IMF}\,(i)$, is defined as

$$f_{\rm IMF}\,(i) \equiv \frac{\displaystyle\int_{M_1}^{M_2} X\,(i,M)\,f_{\rm ej}(M)\,M\,\phi\,(M)\,dM \,/\, X(i)_\odot}{\displaystyle\sum_j \int_{M_1}^{M_2} X\,(j,M)\,f_{\rm ej}(M)\,M\,\phi\,(M)\,dM}, \tag{4·1}$$

where $X(i,M)$ is the mass fraction of the element i in the ejecta, M the initial progenitor mass, $f_{\rm ej}$ the mass ratio of the ejecta to the initial mass and $\phi\,(M) \propto$

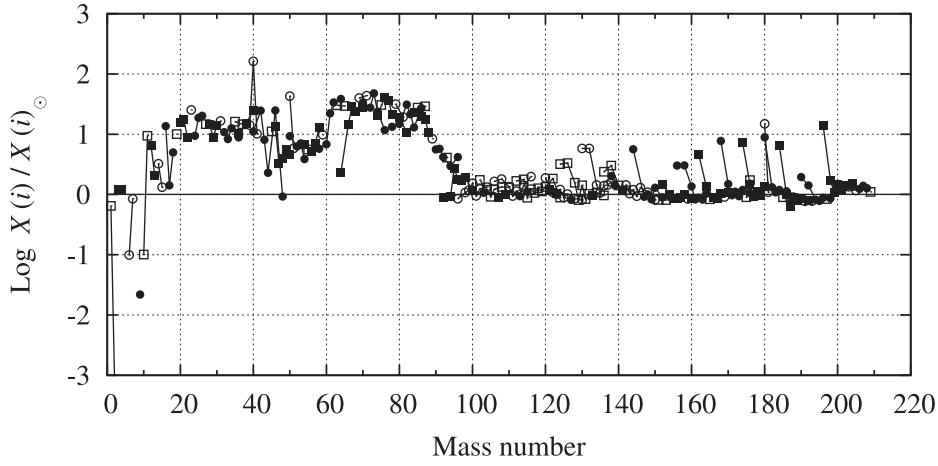

Fig. 12. Same as Fig. 11 but for only from 15 to 40 $M_\odot$.

$M^{-2.35}$ the number of stars within the mass range between M and $M + dM$, which is Salpeter's IMF. Let us adopt spherical postexplosion models from Rauscher et al.[53] for progenitors of 15, 19, 20, 21, 25, 30, 35, and 40 $M_\odot$*) with the solar metallicity and take our model for 70 $M_\odot$. During the integrations in equation (4·1), necessary values of $X(i, M)$ and $f_{\rm ej}$ are obtained by interpolation of sample values. We take M_1 to be 15 $M_\odot$ and M_2 to be 70 $M_\odot$. For our 70 $M_\odot$ model, we assume all of the hydrogen envelope to be ejected as the stellar wind, because 70 $M_\odot$ with the solar metallicity may strongly suffer from the mass loss.[36] Figure 11 shows the IMF averaged overproduction factors. We also show the overproduction factors averaged only from 15 $M_\odot$ to 40 $M_\odot$ in Fig. 12 for reference. We can see relatively high overproduction of ^{40}K relative to the solar value, which arises from the large enhancement of the star of 20 $M_\odot$ (see Fig. 4 in Ref. 53)). We also recognize relatively larger overproduction factors for elements of $60 < A < 90$. The overproduction level of $60 < A < 90$ is slightly enhanced by a few factors due to the inclusion of our 70 $M_\odot$ model (Fig. 11) compared with that averaged over the range only between 15 $M_\odot$ and 40 $M_\odot$ (Fig. 12). Recall that the production of elements of $60 < A < 90$ results from the weak s-process. Overproduced neutron-rich elements of $90 < A < 160$ are attributed to the 70 $M_\odot$ model in which the elements are primarily synthesized in the explosive nucleosynthesis by the r-process. P-elements of $110 < A < 200$ are overproduced to the solar values, which mainly come from the p-process in 15 – 40 $M_\odot$ stars. ^{180}Ta is highly overproduced in our 70 $M_\odot$ model. Therefore, it is interesting whether our model could contribute to the solar ^{180}Ta abundance. If we average the overproduction factors over the mass range only between 15 $M_\odot$ and 40 $M_\odot$ (Fig. 12), the IMF averaged overproduction factor

*) We take the nucleosynthesis data of postsupernova models from the web site: `http://homepages.spa.umn.edu/~alex/nucleosynthesis/RHHW02.shtml`. Note that the data of 30, 35, and 40 $M_\odot$ are not yet published, and necessary data for the integration in Eq. (4·1) are obtained by interpolation.

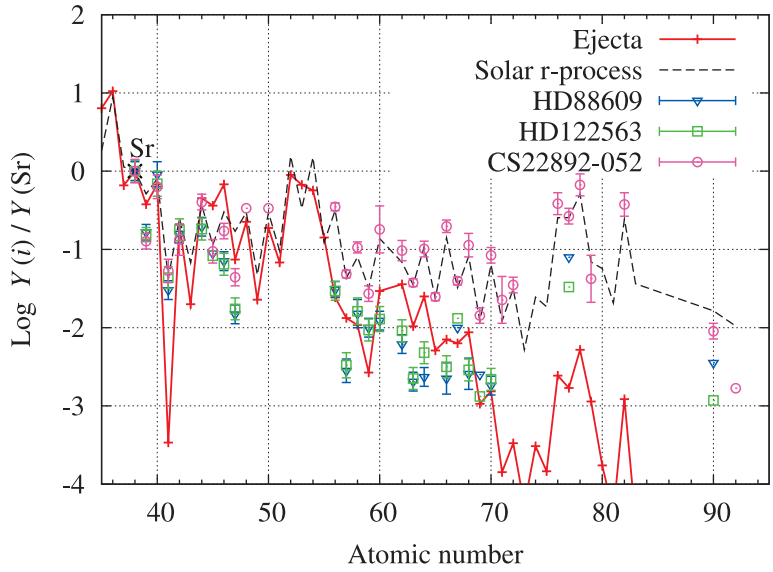

Fig. 13. Abundance ratios relative to Sr: calculated ejecta (solid line), solar system r-process elements (dashed line) (Simmerer et al.[89]) and three very metal-poor stars.[17),90)] Symbols with error bars indicate the observations of their abundances. Triangles, squares and circles represent HD88609, HD122563, and CS22892-052, respectively. Symbols without error bar indicate the upper limits.

of ^{180}Ta is 1.18 in logarithmic scale. On the other hand, if we include the 70 $M_\odot$ model in the integration in Eq. (4·1), the overproduction factor becomes 1.23, which corresponds to a 12% increase. Therefore, the contribution of 40 – 70 $M_\odot$ to the solar ^{180}Ta abundance is negligible in view of uncertainties of the present study. Overall, our model contributes to the solar weak s-elements of $70 < A < 90$ and neutron-rich elements of $90 < A < 160$. However, we should treat the results with caution because our jetlike explosion model is only one specific set of parameters of angular momentum and magnetic field distributions, and the fraction of such an aspherical explosion is highly uncertain. As suggested by Fujimoto et al.,[2)] the r-process does not occur in a less energetic jet and the jet properties depend on specified parameters of the initial angular momentum and magnetic field distributions. If the fraction of jetlike explosions among the progenitors is less than 10%, the contribution of jet-induced nucleosynthesis above 40 $M_\odot$ to the chemical evolution of galaxies would be minor. Therefore, we should regard the contributions of our model deduced here as the upper limits. In addition, we investigate only the progenitors with solar metallicity. As a consequence, some simulations of the chemical evolution of galaxies are required to ascertain the contribution especially for elements whose productions depend on the metallicity, which is beyond the scope of this paper.

4.2. *Comparison with abundances in metal-poor stars and the possibility for LEPP*

Although our progenitor is assumed to have the solar metallicity, the production of r-elements, which are primarily synthesized without seeds, does not depend on the

Table II. Abundance ratios relative to the solar values for extremely metal-poor stars and our model indicated by "Ejecta".

	[Fe/H]	[Sr/Fe]	[Y/Fe]	[Zr/Fe]	[Eu/Fe]	[Sr/Eu]
CS22892-052	−3.1	+0.6	+0.44	+0.78	+1.64	−1.04
HD88609	−3.0	−0.05	−0.12	+0.24	−0.33	+0.28
HD122563	−2.7	−0.27	−0.37	−0.10	−0.52	+0.25
Ejecta	–	+1.50	+1.79	+1.65	+1.90	−0.4

metallicity. Therefore, it is worthwhile to compare our results with the abundances of extremely metal-poor stars, which are not affected seriously by the *s*-process. It is noted that the overproduced elements of $Z > 38$ are primarily produced in the explosive nucleosynthesis. Abundance ratios relative to Sr against the atomic number are shown in Fig. 13. Solid and dashed lines denote abundance ratios of our model and that of solar system *r*-process elements,[89] respectively. Circles, triangles, and squares indicate the values of observations of very metal-poor stars CS22892-052,[17] HD88609[90] and HD122563,[90] respectively. The symbols without error bars indicate the upper limits. We can see that the abundance pattern of CS22892-052, which is a typical *r*-process-rich ([Eu/Fe] $\gtrsim 1$) star, coincides well with that of the solar *r*-element pattern, although some exceptions are recognized. The *r*-process-poor stars ([Eu/Fe] $\lesssim 1$), HD88609 and HD122563, have a clearly decreasing trend as the atomic number increases. It is noted that although [Eu/Fe] values of *r*-process-poor stars are low compared with those of the *r*-process-rich ones, abundances in HD88609 ([Fe/H] ~ -3.0) and HD122563 ([Fe/H] ~ -2.7) should come from the weak *r*-process because the sources of the *s*-process, AGB stars, have not had sufficient time to evolve before the formation of such metal-poor halo stars.[90] The abundances of the ejecta of our model show a decreasing trend in proportion to the decrease in the atomic number, which is similar to the case of HD88609 and HD122563.[16] This result can be attributed to the decrease in the ejected masses at lower values of $Y_{e,f}$ (Fig. 6).

The abundance ratios relative to the solar values are summarized in Table II, where the observational values are taken from Sneden et al.[17] for CS22892-052 and Honda et al.[90] for HD88609 and HD122563. The values of [Sr/Fe], [Y/Fe] and [Zr/Fe] are similarly observed and the ejecta also has the same tendency. While [Sr/Eu] of the *r*-process-rich star CS22892-052 ([Sr/Eu] ~ -1) is very small compared with that of the *r*-process-poor stars HD88609 and HD122563 ([Sr/Eu] $\sim +0.3$), the value of the ejecta ([Sr/Eu] ~ -0.4) is closer to that of the *r*-process-poor stars than to that of the *r*-process-rich stars, which reflects the declining trend of abundances as the atomic number increases (Fig. 13).

We find that Sr-Y-Zr isotopes are primarily synthesized in the explosive nucleosynthesis by a similar process of primary synthesis of light *p*-elements as described in §3.3. The ejected matter of $T_{9,\max} \sim 16$ and $Y_{e,f} \sim 0.45$ produces most isotopes of Sr-Y-Zr, which is more neutron rich than that in the case of primary light *p*-element

synthesis. In such high peak temperature and density, there exist protons, neutrons, and alpha particles, where a lot of neutrons are produced by electron captures. After the temperature decreases to 8×10^9 K, a sequence of neutron captures and β^--decays produces slightly neutron-rich Sr-Y-Zr isotopes from lighter elements. After the exhaustion of neutrons, proton captures and gamma processes follow. Recall that ^{96}Zr is overproduced relative to the solar value in the hydrostatic nucleosynthesis (Fig. 1). ^{88}Sr, ^{89}Y, and ^{91,92,94,96}Zr are highly overproduced relative to the solar values due to the primary process in the explosive nucleosynthesis. It is noted that ^{96}Zr is more produced in the explosive nucleosynthesis.

Travaglio et al.[18] have suggested that based on a galactic chemical evolution (GCE) model, a primary process from massive stars (LEPP) other than the general *s*- and *r*-processes is needed to explain 8% of the solar abundance for Sr and 18% of the solar Y and Zr abundances. In their GCE model, the yields of the *s*-process have been derived from AGB models and they have also added a small contribution ($\sim$ 10% of the solar ones) from the weak *s*-component for Sr. It is emphasized that the contribution from the *r*-process has been deduced from the very *r*-process-rich CS22892-052,[17] that is, contributions to *r*-elements from *r*-process-*poor* stars like our explosion model have not been included. In our explosion model, the ejecta has a larger [Sr/Eu] than that of *r*-process-rich stars, and Sr, Y, and Zr are mainly produced by the primary process. Therefore, our explosion model could be one of the sites of LEPP. However, the calculations are limited to only one model of the progenitor with the solar metallicity and specific set of parameters of initial distribution of magnetic field and angular momentum. As suggested in Ref. 2), ejected masses of *r*-elements depend on the jet properties such as the explosion energies. Therefore, the effects of explosion models on the chemical evolution of galaxies remain uncertain and should be studied in the future.

Acknowledgements

We would like to thank A. Heger and his collaborators for offering their data. M. Ono thanks N. Nishimura for stimulating discussion. K. Kotake is grateful to K. Sato for continuous encouragement. This work has been supported in part by Grants-in-Aid for Scientific Research (Nos. 18540279, 19104006, 20740150, 22540297 and 24540278) from the Ministry of Education, Culture, Sports, Science and Technology of Japan.

Appendix A

—— *Thermal Population of Ground and Isomeric States of* ^{180}Ta ——

^{180}Ta is one of the rarest isotopes in the solar system and it has a long-lived isomeric state. The isomeric state has $J^\pi = 9^-$ and the half-life $\tau_{1/2}$ is 1.2×10^{15} yr, while the ground state has $J^\pi = 1^+$ and $\tau_{1/2} \simeq 8.152$ h. We treat specially the reaction rates concerning ^{180}Ta by a method similar to that described in Ref. 53).

Because of the selection rule for the spin and parity, the isomeric state (^{180m}Ta) cannot directly decay into the grand state (^{180g}Ta). However, if the temperature is

sufficiently high, ^{180m}Ta can decay into the ground state through thermally excited states. In stellar interiors during some burning stages and in supernova explosions, the two states of ^{180}Ta are thermally populated. In thermal equilibrium, the population ratio $P_{\rm iso}$ of the isomer relative to the ground state is given as[53]

$$P_{\rm iso} = \frac{(2J_{\rm iso}+1)\exp(-E_{\rm iso}/kT)}{(2J_{\rm gs}+1)} = \frac{19}{3}e^{-0.8738/T_9}, \qquad (\text{A}\cdot1)$$

where $J_{\rm gs}$ and $J_{\rm iso}$ are the spins of the ground and isomeric states, respectively, and $E_{\rm iso}$ the excitation energy of the isomer, $T_9 = T/10^9$ K. If the temperature decreases to a critical temperature $T_{\rm crit}$, the two states no longer interact with each other. In the explosive burning scenario, the critical temperature is crucial to determine the amount of ^{180m}Ta. Belic et al.[91] have derived the effective decay rate of ^{180m}Ta by photoactivation experiments. We simply assume $T_{\rm crit}$ as 0.35×10^9 K from the temperature-dependent decay rate (Fig. 4 in Ref. 91)). The effective ^{180}Ta rates of neutron-induced reaction and β-decays are given by

$$\lambda_{\rm eff} = f_{\rm gs}\lambda_{\rm gs} + f_{\rm iso}\lambda_{\rm iso}, \qquad (\text{A}\cdot2)$$

where $f_{\rm gs}$ and $f_{\rm iso}$ are the fractions of the ground and isomeric states, respectively. For this effective decay rate, we derive $\lambda_{\rm gs}$ from the half-life of the ground state and $\lambda_{\rm iso}$ from Belic et al.[91] For the neutron capture of ^{180}Ta, $\lambda_{\rm gs}$ is taken from Ref. 53) and $\lambda_{\rm iso}$ is taken from the JINA REACLIB database.[60] If $T < T_{\rm crit}$, we make all the ^{180g}Ta decayed by hand and set $f_{\rm gs}$ to be 0.

References

1) S. Fujimoto, M. Hashimoto, K. Kotake and S. Yamada, Astrophys. J. **656** (2007), 382.
2) S. Fujimoto, N. Nishimura and M. Hashimoto, Astrophys. J. **680** (2008), 1350.
3) F.-K. Thielemann, A. Arcones, R. Käppeli, M. Liebendörfer, T. Rauscher, C. Winteler, C. Fröhlich, I. Dillmann, T. Fischer, G. Martinez-Pinedo, K. Langanke, K. Farouqi, K.-L. Kratz, I. Panov and I. K. Korneev, Prog. Part. Nucl. Phys. **66** (2011), 346.
4) E. M. Burbidge, G. R. Burbidge, W. A. Fowler and F. Hoyle, Rev. Mod. Phys. **29** (1957), 547.
5) R. D. Hoffman, S. E. Woosley and Y.-Z. Qian, Astrophys. J. **482** (1997), 951.
6) K. Otsuki, H. Tagoshi, T. Kajino and S. Wanajo, Astrophys. J. **533** (2000), 424.
7) S. Wanajo, Astrophys. J. **666** (2007), L77.
8) T. Kuroda, S. Wanajo and K. Nomoto, Astrophys. J. **672** (2008), 1068.
9) T. Fischer, S. C. Whitehouse, A. Mezzacappa, F.-K. Thielemann and M. Liebendörfer, Astron. Astrophys. **517** (2010), A80.
10) B. D. Metzger, G. Martínez-Pinedo, S. Darbha, E. Quataert, A. Arcones, D. Kasen, R. Thomas, P. Nugent, I. V. Panov and N. T. Zinner, Mon. Not. R. Astron. Soc. **406** (2010), 2650.
11) L. F. Roberts, D. Kasen, W. H. Lee and E. Ramirez-Ruiz, Astrophys. J. **736** (2011), L21.
12) S. Goriely, A. Bauswein and H.-T. Janka, Astrophys. J. **738** (2011), L32.
13) S. Wanajo and H.-T. Janka, Astrophys. J. **746** (2012), 180.
14) F. Käppeler, R. Gallino, S. Bisterzo and W. Aoki, Rev. Mod. Phys. **83** (2011), 157.
15) M. Rayet, M. Arnould, M. Hashimoto, N. Prantzos and K. Nomoto, Astron. Astrophys. **298** (1995), 517.
16) I. U. Roederer, J. J. Cowan, A. I. Karakas, K.-L. Kratz, M. Lugaro, J. Simmerer, K. Farouqi and C. Sneden, Astrophys. J. **724** (2010), 975.

17) C. Sneden, J. J. Cowan, J. E. Lawler, I. I. Ivans, S. Burles, T. C. Beers, F. Primas, V. Hill, J. W. Truran, G. M. Fuller, B. Pfeiffer and K.-L. Kratz, Astrophys. J. **591** (2003), 936.
18) C. Travaglio, R. Gallino, E. Arnone, J. Cowan, F. Jordan and C. Sneden, Astrophys. J. **601** (2004), 864.
19) L. Wang, J. C. Wheeler, P. Höflich, A. Khokhlov, D. Baade, D. Branch, P. Challis, A. V. Filippenko, C. Fransson, P. Garnavich, R. P. Kirshner, P. Lundqvist, R. McCray, N. Panagia, C. S. J. Pun, M. M. Phillips, G. Sonneborn and N. B. Suntzeff, Astrophys. J. **579** (2002), 671.
20) M. Tanaka, K. Maeda, P. A. Mazzali and K. Nomoto, Astrophys. J. **668** (2007), L19.
21) S. Woosley and T. Janka, Nature Phys. **1** (2005), 147.
22) K. Kotake, K. Sato and K. Takahashi, Rep. Prog. Phys. **69** (2006), 971.
23) K. Kotake, arXiv:1110.5107.
24) K. Kotake, T. Takiwaki, Y. Suwa, W. Iwakami Nakano, S. Kawagoe, Y. Masada and S. Fujimoto, arXiv:1204.2330.
25) K. Kotake, K. Sumiyoshi, S. Yamada, T. Takiwaki, T. Kuroda, Y. Suwa and H. Nagakura, arXiv:1205.6284.
26) A. Marek and H.-T. Janka, Astrophys. J. **694** (2009), 664.
27) Y. Suwa, K. Kotake, T. Takiwaki, S. C. Whitehouse, M. Liebendörfer and K. Sato, Publ. Astron. Soc. Jpn. **62** (2010), L49.
28) T. Takiwaki, K. Kotake and Y. Suwa, arXiv:1108.3989.
29) T. Kuroda, K. Kotake and T. Takiwaki, arXiv:1202.2487.
30) T. Fischer, I. Sagert, G. Pagliara, M. Hempel, J. Schaffner-Bielich, T. Rauscher, F.-K. Thielemann, R. Käppeli, G. Martínez-Pinedo and M. Liebendörfer, Astrophys. J. Suppl. **194** (2011), 39.
31) K. Kotake, H. Sawai, S. Yamada and K. Sato, Astrophys. J. **608** (2004), 391.
32) H. Sawai, K. Kotake and S. Yamada, Astrophys. J. **631** (2005), 446.
33) M. Shibata, Y. T. Liu, S. L. Shapiro and B. C. Stephens, Phys. Rev. D **74** (2006), 104026.
34) Y. Suwa, T. Takiwaki, K. Kotake and K. Sato, Publ. Astron. Soc. Jpn. **59** (2007), 771.
35) T. Takiwaki, K. Kotake and K. Sato, Astrophys. J. **691** (2009), 1360.
36) A. Heger, C. L. Fryer, S. E. Woosley, N. Langer and D. H. Hartmann, Astrophys. J. **591** (2003), 288.
37) A. I. MacFadyen and S. E. Woosley, Astrophys. J. **524** (1999), 262.
38) S. Harikae, K. Kotake, T. Takiwaki and Y. Sekiguchi, Astrophys. J. **720** (2010), 614.
39) I. Zalamea and A. M. Beloborodov, Mon. Not. R. Astron. Soc. **410** (2011), 2302.
40) S. E. Woosley, Astrophys. J. **405** (1993), 273.
41) S. Koide, K. Shibata, T. Kudoh and D. L. Meier, Science **295** (2002), 1688.
42) D. Proga, A. I. MacFadyen, P. J. Armitage and M. C. Begelman, Astrophys. J. **599** (2003), L5.
43) Y. Mizuno, S. Yamada, S. Koide and K. Shibata, Astrophys. J. **615** (2004), 389.
44) S. Fujimoto, K. Kotake, S. Yamada, M. Hashimoto and K. Sato, Astrophys. J. **644** (2006), 1040.
45) S. Nagataki, R. Takahashi, A. Mizuta and T. Takiwaki, Astrophys. J. **659** (2007), 512.
46) S. Harikae, T. Takiwaki and K. Kotake, Astrophys. J. **704** (2009), 354.
47) S. Nagataki, Astrophys. J. **704** (2009), 937.
48) S. Nagataki, Publ. Astron. Soc. Jpn. **163** (2011), 1243.
49) R. D. Blandford and R. Znajek, Mon. Not. R. Astron. Soc. **179** (1977), 433.
50) S. Nagataki, A. Mizuta, S. Yamada, H. Takabe and K. Sato, Astrophys. J. **596** (2003), 401.
51) S. Nagataki, A. Mizuta and K. Sato, Astrophys. J. **647** (2006), 1255.
52) C. Winteler, R. Käppeli, A. Perego, A. Arcones, N. Vasset, N. Nishimura, M. Liebendörfer and F.-K. Thielemann, Astrophys. J. **750** (2012), L22.
53) T. Rauscher, A. Heger, R. D. Hoffman and S. E. Woosley, Astrophys. J. **576** (2002), 323.
54) S. E. Woosley and T. A. Weaver, Astrophys. J. Suppl. **101** (1995), 181.
55) S. Fujimoto, K. Kotake, M. Hashimoto, M. Ono and N. Ohnishi, Astrophys. J. **738** (2011), 61.
56) M. Ono, M. Hashimoto, S. Fujimoto, K. Kotake and S. Yamada, Prog. Theor. Phys. **122** (2009), 755.
57) M. Hashimoto, Prog. Theor. Phys. **94** (1995), 663.

58) J. Puls, J. S. Vink and F. Najarro, Astron. Astrophys. Rev. **16** (2008), 209.
59) N. Prantzos, M. Arnould and J.-P. Arcoragi, Astrophys. J. **315** (1987), 209.
60) R. H. Cyburt, A. M. Amthor, R. Ferguson, Z. Meisel, K. Smith, S. Warren, A. Heger, R. D. Hoffman, T. Rauscher, A. Sakharuk, H. Schatz, F. K. Thielemann and M. Wiescher, Astrophys. J. Suppl. **189** (2010), 240.
61) I. Dillmann, M. Heil, F. Käppeler, R. Plag, T. Rauscher and F.-K. Thielemann, in *Capture Gamma-Ray Spectroscopy and Related Topics*, AIP Conf. Proc. Vol. 819, ed. A. Woehr and A. Aprahamian (2006), p. 123.
62) K. Takahashi and K. Yokoi, At. Data Nucl. Data Tables **36** (1987), 375.
63) E. Anders and N. Grevesse, Geochim. Cosmochim. Acta **53** (1989), 197.
64) N. Langer, J.-P. Arcoragi and M. Arnould, Astron. Astrophys. **210** (1989), 187.
65) M. Rayet and M. Hashimoto, Astron. Astrophys. **354** (2000), 740.
66) M. Arnould, Astron. Astrophys. **46** (1976), 117.
67) K. Nomoto and M. Hashimoto, Phys. Rep. **163** (1988), 13.
68) M. Hashimoto, K. Nomoto and T. Shigeyama, Astron. Astrophys. **210** (1989), L5.
69) J. M. Stone and M. L. Norman, Astrophys. J. Suppl. **80** (1992), 753.
70) J. M. Stone and M. L. Norman, Astrophys. J. Suppl. **80** (1992), 791.
71) K. Kotake, S. Yamada and K. Sato, Astrophys. J. **595** (2003), 304.
72) H. Shen, H. Toki, K. Oyamatsu and K. Sumiyoshi, Nucl. Phys. A **637** (1998), 435.
73) N. Yasutake, K. Kotake, M. Hashimoto and S. Yamada, Phys. Rev. D **75** (2007), 084012.
74) B. Paczyński and P. J. Wiita, Astron. Astrophys. **88** (1980), 23.
75) A. Heger, S. E. Woosley and H. C. Spruit, Astrophys. J. **626** (2005), 350.
76) S. A. Balbus and J. F. Hawley, Rev. Mod. Phys. **70** (1998), 1.
77) M. Obergaulinger, P. Cerdá-Durán, E. Müller and M. A. Aloy, Astron. Astrophys. **498** (2009), 241.
78) T. Piran, Rev. Mod. Phys. **76** (2005), 1143.
79) J. Granot and E. Ramirez-Ruiz, Astrophys. J. **609** (2004), L9.
80) S. Nagataki, M. Hashimoto, K. Sato and S. Yamada, Astrophys. J. **486** (1997), 1026.
81) S. Nishimura, K. Kotake, M. Hashimoto, S. Yamada, N. Nishimura, S. Fujimoto and K. Sato, Astrophys. J. **642** (2006), 410.
82) T. Rauscher and F.-K. Thielemann, At. Data Nucl. Data Tables **75** (2000), 1
83) T. Rauscher and F.-K. Thielemann, At. Data Nucl. Data Tables **79** (2001), 47.
84) S. Goriely, F. Tondeur and J. M. Pearson, At. Data Nucl. Data Tables **77** (2001), 311.
85) P. Möller, J. R. Nix, W. D. Myers and W. J. Swiatecki, At. Data Nucl. Data Tables **59** (1995), 185.
86) M. Rayet, M. Arnould and N. Prantzos, Astron. Astrophys. **227** (1990), 271.
87) W. M. Howard, B. S. Meyer and S. E. Woosely, Astrophys. J. **373** (1991), L5.
88) E. E. Salpeter, Astrophys. J. **121** (1955), 161.
89) J. Simmerer, C. Sneden, J. J. Cowan, J. Collier, V. M. Woolf and J. E. Lawler, Astrophys. J. **617** (2004), 1091.
90) S. Honda, W. Aoki, Y. Ishimaru and S. Wanajo, Astrophys. J. **666** (2007), 1189.
91) D. Belic, C. Arlandini, J. Besserer, J. de Boer, J. J. Carroll, J. Enders, T. Hartmann, F. Käppeler, H. Kaiser, U. Kneissl, M. Loewe, H. J. Maier, H. Maser, P. Mohr, P. von Neumann-Cosel, A. Nord, H. H. Pitz, A. Richter, M. Schumann, S. Volz and A. Zilges, Phys. Rev. Lett. **83** (1999), 5242.